Pressure Sensitive Paint Measurements at High Mach Numbers

H. Zare-Behtash,* K.H. Lo, L. Yang, and K. Kontis

University of Glasgow, School of Engineering, Glasgow G12 8QQ, UK

Abstract

Depending on the case study examined, different PSPs may be used, each applied using a different method onto the model. For polymer PSP the paint is sprayed on. In contrast, the model may first be anodized or covered with a thin-layer chromatography plate and then dipped in PSP. The objective of the present study is to analyse the characteristics of different PSP substrates at high Mach numbers which use two well known PSP molecules: (i) tris-Bathophenanthroline Ruthenium (II) Perchlorate and (ii) Platinum-tetrakis (pentafluorophenyl) Porphyrin. Using a double ramp geometry under a Mach 5 hypersonic flow the feasibility of applying each of the aforementioned PSP methods is investigated and compared to discrete pressure measurements. The flow over a 3D bump under a Mach 1.3 flow is also studied to give a broader Mach number range. In the hypersonic tunnel, all PSP techniques and formulations were able to capture the complex flowfield with the results quantitatively agreeing with the discrete measurements. For the transonic bumps however, it was found that the polymer based Platinum PSP could map the flowfield more accurately.

Keywords: Pressure Sensitive Paint, Thin Layer Chromatography, AA-PSP, Flow Diagnostics

*Hossein.Zare-Behtash@glasgow.ac.uk.

I. INTRODUCTION

The pressure-sensitive paint technique has the capability of providing a global quantitative, non-intrusive measurement of the pressure distribution over large surfaces. Detailed description of the principles of operation of PSP along with its merits over onventional pressure measurement techniques are well documented in the literature.[1–4] Conventional PSP contains luminescent molecules distributed in an oxygen-permeable polymer binder, which is sprayed or painted on the model surface. To increase the emission signal level, a base coat is usually added on the model surface underneath the PSP layer. The polymer based PSP has been successfully applied in low speed,[5,6] transonic,[7–10] supersonic,[11–14] and hypersonic flows.[15–17]

Additionally, porous PSP techniques are also available which increase the response time due to a greater surface area available that increases the chance of interaction of the oxygen molecules in the flow with the PSP molecules.[18] Generally, the thin-layer chromatography (TLC) and anodized aluminium seem to be the most frequently used porous binder for PSP applications in high speed flows. The micropores on the porous binder absorb the luminophore molecules via the internal-molecule force.[16] The open structure of the support matrix makes the oxygen molecule interaction with the luminophores easier. Therefore, fast response time and high pressure sensitivity can be obtained by these paints.

The idea of anodized aluminium PSP (AA-PSP) was initially suggested by Asai et al.[19] and further developed by Sakaue.[20] The luminophore molecules are absorbed into the porous binder structure and interact with the oxygen molecules more easily. The improvement of response time and pressure sensitivity have been successfully recorded at Mach 10.4 flow in a shock tunnel by Nakakita et al.[8,9] Complex flow structures consisting of flow separation, reattachment, and shock-shock interactions were readily captured using the AA-PSP method. A scramjet inlet model coated with AA-PSP was tested in a Mach 4 short duration Ludwieg tube by Sakaue et al.[11] The surface pressure was in the order of hundreds of Pascals and the test duration was around 100 ms. The AA-PSP captured the surface pressure change well and the results agreed with the CFD findings.

Although AA-PSP has been successfully used in the short duration hypersonic tunnels, there are still several limitations of AA-PSP. The model material is limited to pure aluminium or aluminium alloys with small dimensions. For large models with complicated

sensor inside, it is difficult or even impossible to immerse the model in the sulphuric acid solvent for anodization.[21] Mérienne et al.[12] applied an anodized aluminium tape as the PSP binder in the transonic tunnel, where the tape was glued on the model. The fast response is comparable to the Kulite pressure transducers. This is a good idea but it is limited only to 2D geometries, the thickness of the tape must also be take into account.

Another type of porous material used in PSP research are TLC plates. Baron et al.[13] applied TLC as the binder of PSP in a solenoid valve with a pressure jump. The response time of the TLC-PSP can be as low as 10 μs. Sakamura et al.[22] used the TLC-PSP in the shock tube and Laval nozzle testing. The porous PSP captured the shock wave motion in the order of kilohertz during the starting process of the supersonic nozzle in a qualitative manner. TLC-PSP was also applied in the shock tube by Gongora-Orozco et al.[15] The greatest drawback of TLC plates is their fragile surface texture which makes them susceptible to strong interactions and difficult to apply to curved surfaces.

The present study aims to provide a comparison of the changes and differences observed when using the various permutations of the PSP techniques, under high Mach numbers, by applying them to hypersonic and transonic flows. This work builds upon the static tests of Quinn et al.[18]

II. PSP SAMPLES TESTS

The PSP luminophores employed in the present study are the tris-Bathophenanthroline Ruthenium Perchlorate (referred to here as $Ru(dpp)_3$) and the Platinum Tetrakis (pentafluorophenyl) Porphyrin (referred to here as PtTFPP).

A. Polymer PSP

The polymer paint is an in-house developed formulation consisting of Methyl Triethoxysilane (MTEOS), ethanol, and hydrochloric acid (HCl), where MTEOS is the sol-gel binder and ethanol and HCl are the solvents.[23] The polymer-based samples are prepared on 10×10 mm square aluminium plates with a thickness of 1 mm. The samples are first sprayed with a base coat using a white acrylic paint (Ambersil matt Ral9010) with 3 layers. The white base coat reflects the emission and increases the signal level. The polymer paint is applied

on the sample surface using an air brush. The samples are coated with a total of 16 layers. Afterwards, the samples are cured in an oven at 70 degrees for 7 hours to evaporate the solvent in order to obtain a uniform layer of PSP coating.

B. Anodized Aluminium PSP (AA-PSP)

AA-PSP samples are prepared by the anodization procedure proposed by Sakaue[17] with a slight modification. A 1 mm thick aluminium sheet with a length of 150 mm is dipped in a sulphuric acid solution with 1 M concentration at room temperature, instead of the constant low temperature as recommended by Sakaue[17] and Kameda et al.[24] The obtained anodized sheet is then dried and cut into 10×10 mm squares samples.

After anodization the sample is dipped in the porous luminophore solution with a concentration of 0.3 mM/L with respect to the volume of solvent as suggested by Gregory et al.[16] In the case of AA-PSP, dichloromethane (DCM) is used as the solvent.

C. TLC Plate

TLC plates consist of a thin layer of adsorbent material applied over a flat carrier sheet. They are typically used to separate mixtures using the capillary action. Their porous surface provides an ideal environment for the PSP luminophores, increasing the probability of oxygen quenching occurring. A 10×10 mm sample is cut from the TLC silica gel aluminium plate (MERCK Chemicals International). The sample is dipped in the same luminophore solution used in the preparation of AA-PSP.

D. PSP Calibration Statistics

All the static samples (no flow) were simultaneously tested in a sealed calibration chamber by Quinn et al.[18] where pressure and temperature can be controlled; some of their findings are presented here for completeness. A total of six samples were placed in the calibration chamber: the PtTFPP-polymer, PtTFPP-AA-PSP, and PtTFPP-TLC, $Ru(dpp)_3$-polymer, $Ru(dpp)_3$-AA-PSP, and $Ru(dpp)_3$-TLC. According to the findings of Quinn et al.[18] the polymer based paints gave the strongest signal followed by the TLC plate. The AA-PSP

signal was the lowest. This is mainly due to the higher concentration of luminophore accumulated on the model surface for the polymer based PSP, compared to the AA-PSP that is dipped. Additionally, it appears that the TLC plate is a stronger adsorbent than the AA-PSP, therefore more luminophores adhere to the surface. Compared to the PtTFPP luminophore, the $Ru(dpp)_3$ was found to give a higher signal output. The reason for this behaviour is attributed to the higher quantum yield of $Ru(dpp)_3$ compared to PtTFPP.

Generally, it was found that the porous PSP samples (TLC and AA-PSPs) showed a non-linear relationship with pressure change across the sub-atmospheric pressure regime. At the sub-atmospheric pressure conditions, the pressure-sensitivity was the highest showing the suitability of applying porous PSP techniques in supersonic or hypersonic flow conditions where low freestream pressures are encountered. Comparing the two different luminophores, the polymer PtTFPP was found to show a higher pressure sensitivity than the polymer $Ru(dpp)_3$.

III. WIND TUNNEL TESTS

A. Hypersonic Tunnel

The hypersonic facility used is an intermittent blow-down tunnel having a test time of 7.5 seconds, capable of generating flows with a range of Mach numbers from 4 to 6. For the present study a Mach 5 contoured nozzle with an exit diameter of 152 mm is used. The wind tunnel test section is free-jet type having dimensions of 325×325×900 mm (height×width×length). Two 195 mm diameter Quartz windows are installed at the two sides of the test section to provide optical access for flow visualisation.

Unit Reynolds numbers of $4.5\times10^6 m^{-1}$ to $13.5\times10^6 m^{-1}$ can be obtained by varying the supply pressure and heater temperature. The wind tunnel was calibrated and the variation of Mach number and Unit Reynolds number were found to be ±0.4% and ±(3.7 to 3.9)%, respectively. The total pressure and total temperature are monitored using a pitot tube and a thermocouple in the setting chamber upstream of a honeycomb. The outputs from the pressure transducers and thermocouple are recorded using a National Instruments (NI) SXCI-1000 unit and PCI-6251 acquisition card which is controlled using LabVIEW. Further details of the facility and testing instruments, used in this investigation, have been reported

elsewhere.[26,27]

The feasibility and characteristics of the PSP techniques are investigated over a double ramp model in the hypersonic tunnel. The significantly low pressures of the freestream and the relatively large pressure changes expected over the double ramp, due to the compression shocks, are believed to provide a suitable testing case for the PSP techniques.

The dimensions of the aluminium double ramp model investigated are shown in Figure 1. The angle of the first ramp is 12 degrees and the second ramp is 22 degrees relative to the horizontal. The ramp is followed by a 40 mm long flat shoulder with a height of 23.5 mm. Eight pressure taps are incorporated along the model centreline with their locations from the leading edge shown in the figure. These pressure taps are connected to eight Kulite pressure transducers (model XTE-190M, 0-0.7 bar). The pressure data obtained is used for in-situ calibration of the PSPs and for validation of the PSP data. The model is supported by a rigid sting from the back.

The application of PSP to the double ramp model is identical to the preparation procedure of the PSP samples used for pressure and temperature sensitivity analysis and will be detailed in the following section.

B. Trisonic Tunnel

The trisonic wind tunnel is an intermittent indraft wind tunnel, meaning that the airflow inside it is maintained by means of a pressure difference between the atmosphere and a vacuum tank. The test section has dimensions of 150×216×485mm (width×height×length). The wind tunnel test section is situated ahead of a quick operating butterfly valve. When the vacuum tanks are evacuated, the valve is used to open the link between the wind tunnel and the vacuum tanks. When the valve is opened, a pressure difference between the atmosphere and vacuum develops and the air in front of the dryer is sucked inside the vacuum tanks, thus maintaining the air flow inside the tunnel.

The flow Mach number is calculated from the ratio between the total pressure upstream and the total pressure at the test section location.[28] The pressure is recorded via two Kulite XT-190M pressure transducers. Data is collected using a National Instruments (NI) Data Acquisition (DAQ) system, controlled by LabVIEW, at a rate of 20kHz over a 10 second period. The tunnel has a stable run time of approximately 4.5 seconds with a flow Mach

number of 1.3. For the same initial conditions the tunnel exhibits a variation of Mach number of ± 0.01.

Dimensions of the 3D bump employed in this study are given in Figure 2. The maximum height of the bump at its apex is 10 mm. The shape of the bump is similar to that adopted by Byun et al.[29] and is chosen to provide an intricate flowfield to compare the performance of the PSPs.

C. Schlieren Visualisation

Toepler's z-type Schlieren photography[30] is employed to visualise the induced flowfield within the hypersonic tunnel. The system consists of a Palflash 501 continuous light source, two 20.3 cm parabolic mirrors with 208.8 cm focal length and a digital Canon SLR camera. The optical setup is identical to that used by Yang et al.[31] and only a brief description is given here. Colour images are acquired by placing a horizontal 'tricolour' filter at the focal point of the second mirror. A digital Cannon SLR camera, EOS-450D, is used to capture the images, which has a resolution of 12 Mega pixels. The camera is set to continuous shooting mode at a frame rate of 3.5 images per second and the shutter speed is set to the minimum of 1/4000 seconds.

IV. RESULTS AND DISCUSSIONS

A. Double Ramp Model

All PSP experiments are conducted in a dark environment. Two sets of LED panels were used for exciting the PSP. For the $Ru(dpp)_3$ paints blue LEDs with peak wavelength of 475 nm and for the PtTFPP UV LED panels with a peak wavelength of 395 nm were used. A combination of a 530 nm long-pass filter and an infrared cut-off filter was placed in front of a CCD camera to capture the emitted intensity.

The reference image is taken at a known pressure after each test. A dark compensation is performed by subtracting a dark image from the test images. The test image is registered with the correlated reference image using a pixel to pixel registration method to correct any misalignments due to model movement during a test run. The intensity ratio is then obtained by dividing the registered reference and test image. The images were captured at 9

fps frame rate with 10 μs exposure time during the tests. The intensity ratio is converted to a pressure ratio using an in-situ calibration to reduce the influence of temperature variation on paint calibration. A total of 30 images were summed and taken average for processing in order to improve the signal-to-noise-ratio of the data.

In-situ calibration is obtained by relating the Kulite pressure measurement in the test duration and the corresponding PSP intensity at the immediate vicinity of the transducer tappings. The data is fitted with a suitable curve. The advantage of in-situ calibration is that it can eliminate the systematic error caused by the temperature rising in the test duration.

Figure 3 shows the in-situ Stern-Volmer plots of the $Ru(dpp)_3$-TLC, $Ru(dpp)_3$-AA-PSP, $Ru(dpp)_3$-polymer and the PtTFPP-polymer paints. The x-axis is the pressure ratio with respect to the reference pressure and the y-axis is the intensity ratio. Since the experiments are conducted at different runs, the reference conditions are different for each case, as stated in the figure caption. An accurate curve fit can be seen from the plot and each of the calibration curves is applied for the intensity ratio conversion. The curve fits are in the form of:

$$\frac{I_{ref}}{I} = A + B\frac{P}{P_{ref}} + C\left(\frac{P}{P_{ref}}\right)^2 \tag{1}$$

where I_{ref} is the luminescence intensity at the reference pressure P_{ref}. A, B, and C are the constants extracted from curve fitting.

Figure 4 shows the normalised pressure distribution over the double ramp model at an incidence angle of 0 degrees, obtained from the various PSP techniques. These are compared with the flow structures visualised through colour schlieren in Figure 4(a). An interesting finding was that only a very small amount of the Platinum luminophores was adsorbed onto the anodized and TCL models. This led to extremely low signal levels, therefore only the results for the PtTFPP-polymer PSP are presented in Figure 4(e). The reason for this is still unclear. The leading edge shock and the reattachment shock wave are well captured. The thick boundary layer formed downstream of the flow reattachment may indicate the transition in the downstream. The expansion fan is also observable at the corner of the shoulder. The separation shock however, due to its weak nature, is not clearly evident in the figure. The pressure of the PSP images is normalised using the free stream pressure. Due to the nature of the double ramp geometry, the incoming flow is compressed by the

generated leading edge shock wave and the direction of the flow is made parallel to the model surface. The flow separates before encountering the second ramp and re-attaches on the ramp surface. Because of the existence of the separation region, a separation shock wave is generated in front of the separation zone. Downstream of the flow attachment, the transition of the flow may be induced.

Generally, the PSPs are successful in capturing the pressure field over the model surface. Low pressure appears on the first ramp whilst a higher pressure occurs on the second ramp surface because of the compression of the reattachment shock wave. The lowest pressure is visible on the shoulder due to the expansion wave. Compared to the polymer $Ru(dpp)_3$ in Figure 4(b), the porous PSPs, $Ru(dpp)_3$-TLC and $Ru(dpp)_3$-AA-PSP in Figures 4(c) and (d), are capable of capturing the surface flow pressure with more detail. Features such as the separation line and the flow spillage due to the three dimensionality of the flow are much easier to discern through the $Ru(dpp)_3$-TLC and $Ru(dpp)_3$-AA-PSP. The streaks visible on the second ramp are believed to be caused by Görtler vortices present after the flow re-attachment on the second ramp. Alternatively, the polymer PtTFPP in Figure 4(e) is also capable of capturing these vortices. Regions between two adjacent Görtler vortices are characterised by higher pressures since the flow is impinging on the surface. At the same time, where adjacent vortices move the flow away from the model surface results in the occurrence of lower pressure.[32]

The theoretical prediction of the pressure distribution over the double ramp surface is compared with the pressure measurements using $Ru(dpp)_3$-TLC, $Ru(dpp)_3$-AA-PSP, and polymer $Ru(dpp)_3$ in Figure 5. The x-axis starts from the leading edge of the test model and is non-dimensionalised with the the total length of the model (L). Results from the PSP measurements agree well with the transducer measurements. The discrepancy between the theoretical and experimental data at the junction between the first and second ramp, X/L=0.35, is due to the separation of the flow. The same discrepancy also appears around the corner between the second ramp and the flat shoulder at X/L=0.65. Generally, the PSP measurements show higher pressures compared to the Kulite transducers and the theoretical prediction, which is mainly because of the surface temperature rising on the ramp surface especially around the leading edge. This behaviour is evident on all the PSP techniques.

Comparing the $Ru(dpp)_3$-polymer and PtTFPP-polymer paints in Figure 6 leads to the conclusion that PtTFPP PSP has a smoother signal and a better accuracy at lower pressures

up to X/L=0.4. At higher pressures, X/L=0.4 to 0.65, both paints exhibit a similar accuracy. However, as the pressure drops, the PtTFPP has the better correlation with the transducer measurement at X/L=0.7. The smoother signal captured by the PtTFPP-polymer paint is due the difference in the viscosity of the paint compared to the $Ru(dpp)_3$-polymer formulation. The $Ru(dpp)_3$-based paint had a higher viscosity, therefore when using an airbrush to apply the paint on the model it is difficult to achieve a very fine mist in which to obtain a smooth surface finish. This difference can be observed when comparing Figures 4(b) and (e).

Taking the Kulite pressure transducer recordings as the true values, Table I provides the percentage difference between the pressure transducer measurements and the values obtained through the various PSP formulations and methods. In all location the difference between the PSP results and pressure transducer readings was found to be less than 10%. The greatest difference is found in location 6, corresponding to the shoulder of the ramp. The reason for this is attributed to the non-ideal smooth coating of the PSP leading to a very noisy signal. Another reason for the large discrepancy between the discrete pressure measurements and the PSP findings is the dramatic reduction in temperature over the ramp shoulder in transducer location 6. Due to the expansion of the flow over the corner of the shoulder, the temperature drops, and as discovered in previous studies[18] the PSPs exhibit lower pressure sensitivity.

B. 3D Bump

Figure 7 compares the oil flow pattern obtained for the flow over the bump with three different PSP techniques of AA-PSP $Ru(dpp)_3$, polymer $Ru(dpp)_3$, and polymer PtTFPP. Due to the 3D nature of the bump it is not possible to cover the model with TLC plates, highlighting the setback of using TLC plates for PSP. Due to the shape of the bump, the leading portion acts as a ramp, hence the pressure over the leading portion of the bump is expected to be high. As the flow travels over and around the apex flow separation occurs. This creates a pair of counter rotating vortices behind the apex of the bump. Although the PSP results are not calibrated at this stage, due to the relationship between pressure and intensity regions of low intensity ratio correspond to regions of low pressure whereas regions of higher intensity ratio correspond to areas of higher pressure.

All the PSP data was recorded with an identical setup. The only change was the swapping of the blue LEDs for the UV LEDs when conducting experiments with PtTFPP. As visible from Figure 7(b) because the AA-PSP is merely the model dipped in a bath of PSP without having a uniform base coat, like the polymer PSPs, the machining marks over the model surface are readily visible. Due to the complex nature of the model, even though the model surface may be very smooth, when taking high resolution images for PSP the tooling marks left behind make it very difficult to obtain an accurate pixel to pixel alignment when dividing with the reference image. However, the AA-PSP $Ru(dpp)_3$ is still capable of differentiating the high pressure region over the bump and the pressure drop due to the vortex pair at the separation region after the apex of the bump. The polymer $Ru(dpp)_3$ in Figure 7(c), although exhibiting a high signal and a uniform surface, shows an asymmetric pressure pattern which does not seem to corroborate well with the oil flow or AA-PSP findings. The most clear picture of the pressure map relates to the polymer PtTFPP of Figure 7(d). The PtTFPP clearly captures the low pressure regions relating to the two counter rotating vortices as well as the separation line after the apex of the bump.

V. CONCLUSIONS

Various PSP techniques were investigated in a calibration chamber and also on various models in a hypersonic and transonic flow to investigate the effect of binder and luminophore on the pressure and temperature sensitivity as well as their photodegradation rate. Two well known luminophores were adopted in the recipes, $Ru(dpp)_3$ and PtTFPP. It can be concluded that the TLC based PSP has a higher pressure sensitivity compared to the AA-PSP at low pressures but exhibits a lower pressure sensitivity at pressures above atmospheric.

The feasibility of the various PSP techniques were studied by applying them to a double ramp model in a Mach 5 hypersonic flow and a 3D bump in a Mach 1.3 transonic flow. The complex flow patterns were captured by the PSP techniques, such as separation regions, flow re-attachment, and vortices. The measured data agreed well quantitatively with the discrete pressure transducer data. The polymer PtTFPP PSP provided the most consistent performance in both wind tunnel test cases with the polymer $Ru(dpp)_3$ showing the least spatial resolution.

Every PSP recipe has its own particular characteristics in terms of pressure sensitivity,

response time, temperature sensitivity, photodegradation etc. and different research groups use different formulations. Therefore, extending the observations made here to a more global conclusion requires the study of more Mach numbers and perhaps different models to identify which PSP method and luminophore is the most optimum.

Acknowledgments

The support of the EPSRC Engineering Instrument Pool for the loan of the spectrometer is acknowledged. The authors are grateful to Prof. Qin of Sheffield University for supplying the 3D bump contour. Scholarship from the 'UK/China scholarship for excellence' is also greatly appreciated.

---

[1] Bell, J.H., Schairer, E.T., Hand, L.A., Mehta, R.D., "Surface pressure measurements using luminescent coatings," *Annual Review of Fluid Mechanics* **33**, pp. 155–206, 2001.

[2] Zare-Behtash, H., Gongora-Orozco, N., Kontis, K., Holder, S.J., "Application of novel pressure-sensitive paint formulations for the surface flow mapping of high-speed jets," *Experimental Thermal and Fluid Science* **33**, pp. 852–864, 2009.

[3] Carroll, B.F., Abbitt, J.D., Lukas, E.W., Morris, M.J., "Step response of pressure-sensitive paints," *AIAA Journal* **34**, pp. 521–526, 1996.

[4] Moshasrov, V., Radchenko, V., Fonov, S., "Luminescent Pressure Sensors in Aerodynamic Experiments," *Central Aerodynamic Institute (TsAGI)*, 1998.

[5] Schütte, A., Rein, M., Höhler, G., "Experimental and numerical aspects of simulating unsteady flows around the X-31 configuration," *Proceedings of the Institution of Mechanical Engineers, Part G: Journal of Aerospace Engineering* **223**, pp. 309–321, 2009.

[6] Engler, R.H., Mérienne, M.C., Klein, C., Le Sant, Y., "Application of PSP in low speed flows," *Aerospace Science and Technology* **6**, pp. 313–322, 2002.

[7] Watkins, A.N., Buck, G.M., Leighty, B.D., Lipford, W.E., Oglesby, D., "Using pressure- and temperature-sensitive paint on the aftbody of a capsule vehicle," *AIAA Journal* **47**, pp. 821–829, 2009.

[8] Nakakita, K., Yamazaki, T., Asai, K., Fuji, A., "Pressure Sensitive Paint Measurement in

a Hypersonic Shock Tunnel," *21st AIAA Aerodynamic Measurement Technology and Ground Testing Conference*, Colorado, AIAA-2000-2523, 2000.

[9] Nakakita, K., Asai, K., "Pressure-Sensitive Paint Application to a Wing-Body Model in a Hypersonic Shock Tunnel," *22nd AIAA Aerodynamic Measurement Technology and Ground Testing Conference*, Missouri, AIAA-2002-2911, 2002.

[10] Kontis, K., Lada, C., Zare-Behtash, H., "Effect of dimples on glancing shock wave turbulent boundary layer interactions," *Shock Waves* **17**, pp. 323–335, 2008.

[11] Sakaue, H., Matsumura, S., Schneider, S.P., Sullivan, J.P. "Anodized Aluminum Pressure Sensitive Paint for Short Duration Testing," *22nd AIAA Aerodynamic Measurement Technology and Ground Testing Conference*, Missouri, AIAA-2002-2908, 2002.

[12] Mérienne, M.C., Le Sant, Y., Ancelle, J., Soulevant, D., "Unsteady pressure measurement instrumentation using anodized-aluminium PSP applied in a transonic wind tunnel," *Measurement Science and Technology* **15**, pp. 2349–2360, 2004.

[13] Baron, A.E., Danielson, J.D.S., Gouterman, M., Wan, J.R., Callis, J.B., McLachlan B., "Submillisecond response times of oxygen-quenched luminescent coatings," *Review of Scientific Instruments* **64**, pp. 3394–3402, 1993.

[14] Taghavi, R., Raman, G., Bencic, T., "Pressure sensitive paint demonstrates relationship between ejector wall pressure and aerodynamic performance," *Experiments in Fluids* **26**, pp. 481–487, 1999.

[15] Gongora-Orozco, N., Zare-Behtash, H., Kontis, K., "Global unsteady pressure-sensitive paint measurements of a moving shock wave using thin-layer chromatography," *Measurement* **43**, pp. 152–155, 2010.

[16] Gregory, J.W., Asai, K., Kameda, M., Liu, T., Sullivan, J.P., "A review of pressure-sensitive paint for high-speed and unsteady aerodynamics," *Proceedings of the Institution of Mechanical Engineers, Part G: Journal of Aerospace Engineering* **222**, pp. 249–290, 2008.

[17] Sakaue, H., "Luminophore application method of anodized aluminum pressure sensitive paint as a fast responding global pressure sensor," *Review of Scientific Instruments* **76**, pp. 1–8, 2005.

[18] Quinn, M.K., Yang, L., Kontis, K., "Pressure-sensitive paint: effect of substrate," *Sensors* **11**, pp. 11649–11663, 2011.

[19] Asai, K., Kanda, H., Cunningham, C.T., Erausquin, R., Sullivan, J.P., "Surface pressure measurement in a cryogenic wind tunnel by using luminescent coating," *Instrumentation in*

Aerospace Simulation Facilities, Piscataway, pp. 105–114, 1997.

[20] Sakaue, H., Sullivan, J.P., "Time response of anodized aluminum pressure-sensitive paint," *AIAA Journal* **39**, pp. 1944–1949, 2001.

[21] Zare-Behtash, H., Yang, L., Kontis, K., Jones, A., "Anodized aluminium pressure sensitive paint: Effect of paint application technique," *Measurement* **45**, pp. 1902-1905, 2012.

[22] Sakamura, Y., Matsumoto, M., Suzuki, T., "High frame-rate imaging of surface pressure distribution using a porous pressure-sensitive paint," *Measurement Science and Technology* **16**, pp. 759–765, 2005.

[23] Gongora-Orozco, N., Zare-Behtash, H., Kontis, K., "Effects of filters on the performance and characteristics of pressure-sensitive paints," *Measurement Science and Technology* **20**, pp. 077004, 2009.

[24] Kameda, M., Tabei, T., Nakakita, K., Sakaue, H., Asai, K., "Image measurements of unsteady pressure fluctuation by a pressure-sensitive coating on porous anodized aluminium," *Measurement Science and Technology* **16**, pp. 2517–2524, 2005.

[25] Brown, O.C., "Low-speed pressure measurements using a luminescent coating system," *PhD Thesis*, Stanford University, 2000.

[26] Erdem, E., Kontis, K., "Numerical and experimental investigation of transverse injection flows," *Shock Waves*, **20**, pp. 103-118, 2010.

[27] Erdem, E., Yang, L., Kontis, K., "Drag Reduction Studies by Steady Energy Deposition at Mach 5," *49th AIAA Aerospace Sciences Meeting including the New Horizons Forum and Aerospace Exposition*, Orlando, AIAA-2011-1027, 2011.

[28] Pope, A., Goin, K.L., "High-Speed Wind Tunnel Testing," *Krieger*, 1978.

[29] Byun, G., Simpson, R.L., Long, C.H., "Study of vortical separation from three-dimensional symmetric bumps," *AIAA Journal* **42**, pp. 754–765, 2004.

[30] Settles, G.S., "Schlieren and shadowgraph techniques: visualizing phenomena in transparent media," *Springer Verlag*, 2001.

[31] Yang, L., Zare-Behtash, H., Erdem, E., Kontis, K., "Application of AA-PSP to hypersonic flows: the double ramp model," *Sensors and Actuators B* **161**, pp. 100–107, 2012.

[32] Yang, L., Zare-Behtash, H., Erdem, E., Kontis, K., "Investigation of the double ramp in hypersonic flow using luminescent measurement systems," *Experimental Thermal and Fluid Science* **40**, pp. 50-56, 2012.

TABLE I: Percentage difference between pressure taps and various PSPs for the double ramp.

	Pressure Tap Location					
	1	2	3	4	5	6
$Ru(dpp)_3$-Polymer	4.50	4.39	0.48	0.72	1.38	115.56
$Ru(dpp)_3$-AA-PSP	3.97	7.09	9.69	0.01	0.33	7.66
$Ru(dpp)_3$-TLC	2.61	8.97	9.43	0.76	0.13	64.09
PtTFPP-Polymer	1.28	4.24	6.04	0.22	2.49	22.99

List of Figures

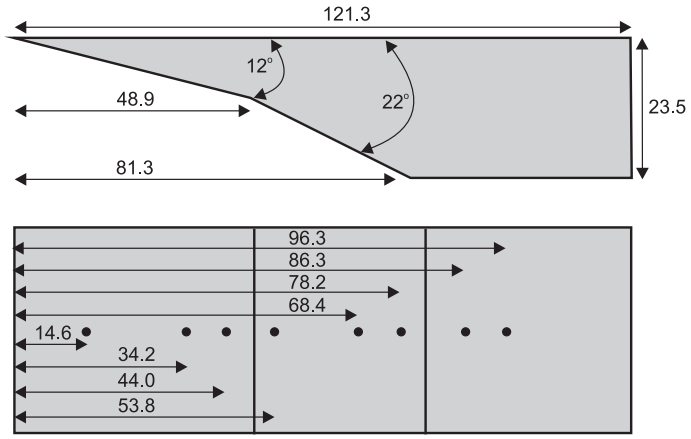

FIG. 1: Model geometry and pressure tapping locations for the double ramp (dimensions in mm).

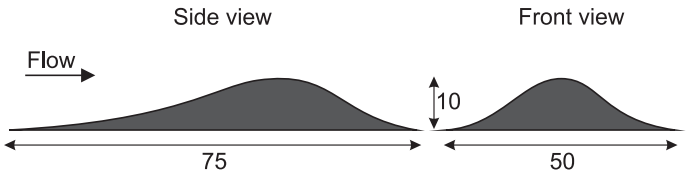

FIG. 2: 3D bump geometry (dimensions in mm).

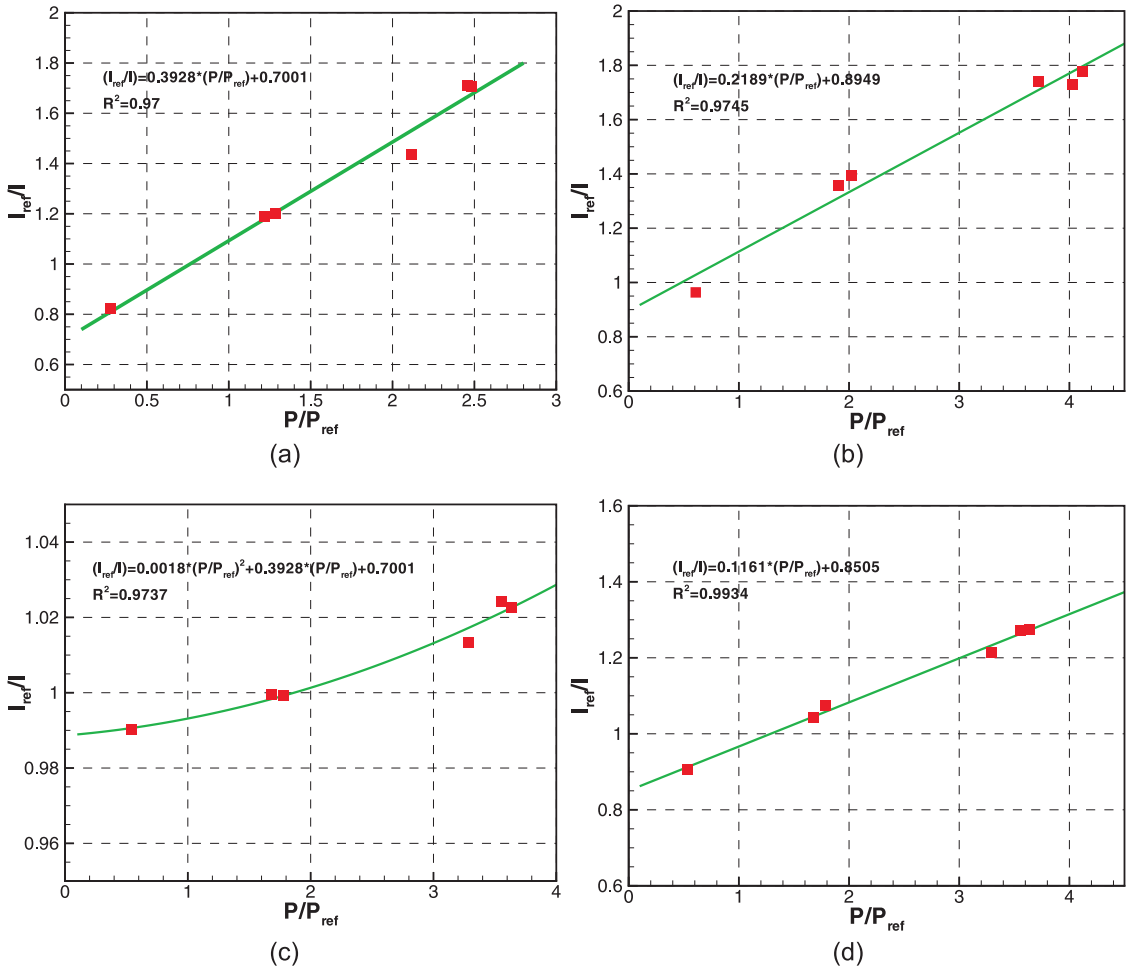

FIG. 3: In-situ calibration curves of: (a) Ru(dpp)$_3$-TLC at reference pressure 4.11 kPa, (b) Ru(dpp)$_3$-AA-PSP at reference pressure 2.52 kPa, (c) Ru(dpp)$_3$)-polymer at reference pressure 2.82 kPa, (d) PtTFPP-polymer at reference pressure 2.82 kPa.

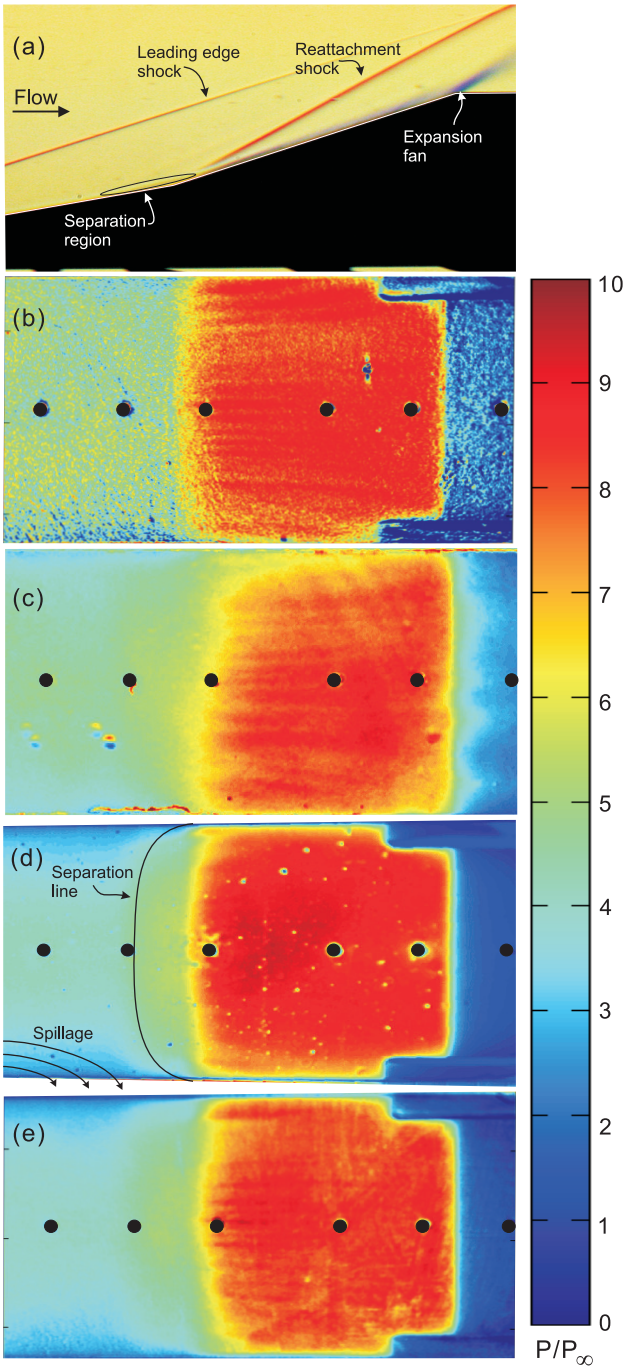

FIG. 4: Comparison of flow patterns depicted by: (a) colour Schlieren, (b) $Ru(dpp)_3$-polymer , (c) $Ru(dpp)_3$-TLC , (d) $Ru(dpp)_3$-AA-PSP, (e) PtTFPP-polymer.

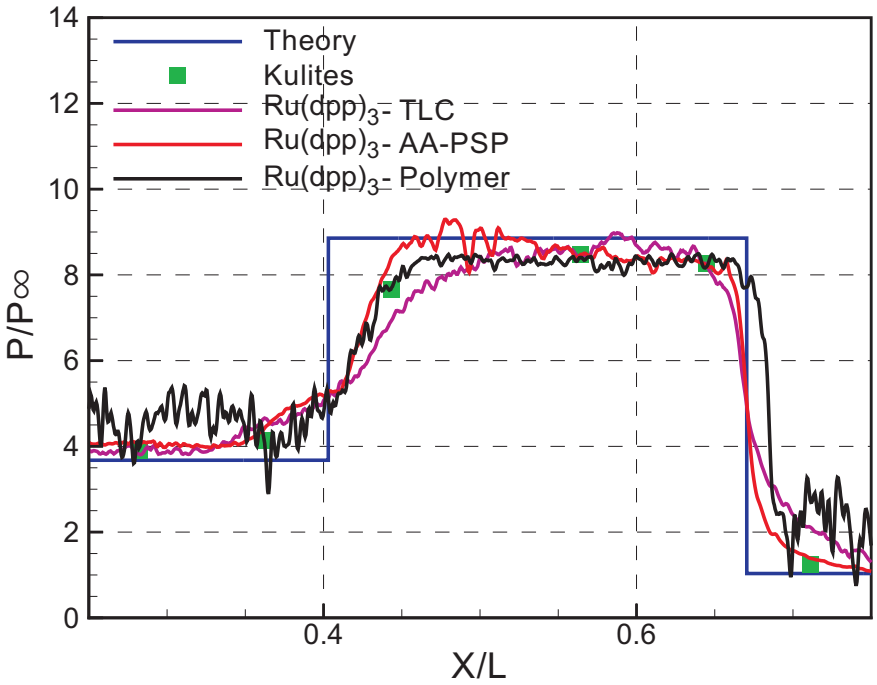

FIG. 5: Comparison of the centreline pressure profile from the theoretical analysis with $Ru(dpp)_3$-polymer, $Ru(dpp)_3$-TLC, and $Ru(dpp)_3$-AA-PSP.

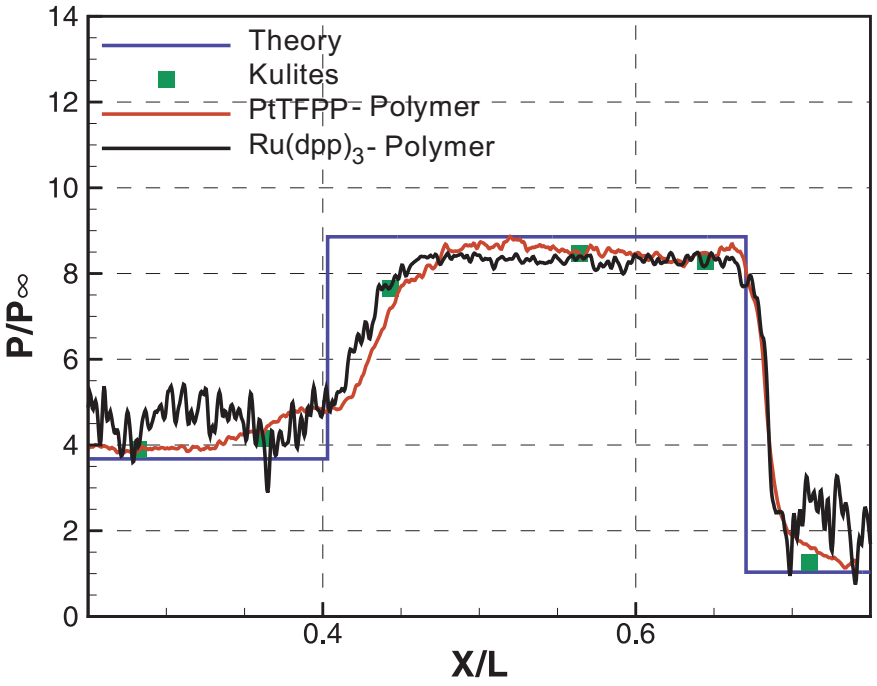

FIG. 6: Comparison of centreline pressure profile from the theoretical analysis with $Ru(dpp)_3$-polymer and PtTFPP-polymer.

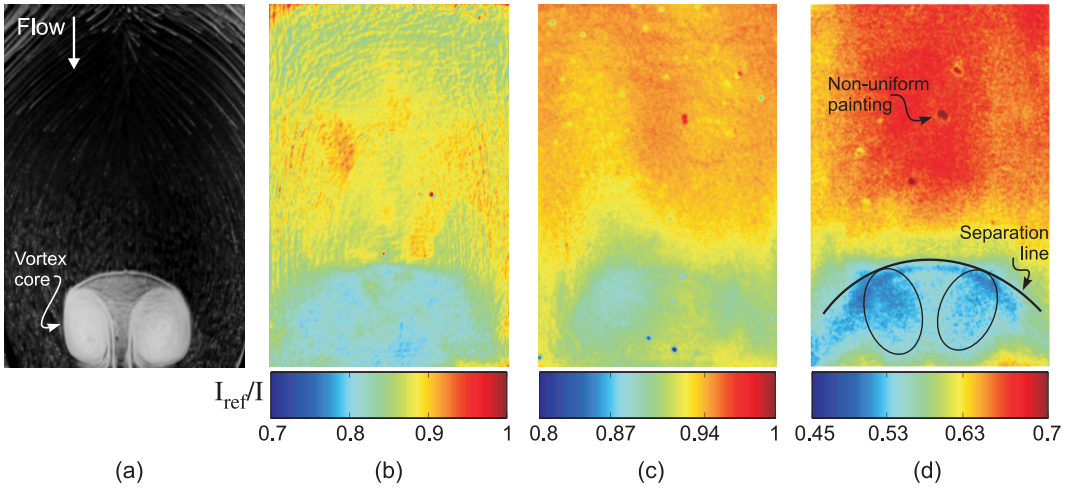

FIG. 7: Comparison of flow patterns over the 3D bump as depicted by: (a) oil flow, (b) $Ru(dpp)_3$-AA-PSP, (c) $Ru(dpp)_3$-polymer, (d) PtTFPP-polymer.